Journal of Inflammation Research

Dovepress
Taylor & Francis Group

Open Access Full Text Article

ORIGINAL RESEARCH

Exploration of Immune-Related Transcription Control/Regulation in Intracranial Aneurysm Through KEGG Analysis and in-vivo Validation

Jianjun Huang[1,*], Shuya Gao[2,*], Shunli Liu[2], Li Liu[3,4]

[1]Department of Neurology, Affiliated Hospital of Youjiang Medical University for Nationalities, Youjiang Medical University for Nationalities, Baise, Guangxi, 533000, People's Republic of China; [2]Graduate School of Youjiang Medical University for Nationalities, Baise, Guangxi, 533000, People's Republic of China; [3]Youjiang Medical University for Nationalities, Affiliated Hospital of Youjiang Medical University for Nationalities, Baise, Guangxi, 533000, People's Republic of China; [4]Laboratory of the Atherosclerosis and Ischemic Cardiovascular Disease, Affiliated Hospital of Youjiang Medical University for Nationalities, Baise, 533000, People's Republic of China

*These authors contributed equally to this work

Correspondence: Li Liu, Youjiang Medical University for Nationalities, Affiliated Hospital of Youjiang Medical University for Nationalities, No. 98 Chengxiang Road, Youjiang District, Baise, Guangxi, 533000, People's Republic of China, Email liuli011258@sina.com

Background: Intracranial aneurysms (IAs), a leading cause of subarachnoid hemorrhage, rank second only to cerebral thrombosis and hypertensive intracerebral hemorrhage among cerebrovascular diseases. However, the understanding of the regulatory mechanisms associated with IAs remains limited currently.

Methods: We obtained the GSE122897 dataset and analyzed differential expression genes (DEGs) from control, Ruptured intracranial aneurysm (RIA) and Unruptured intracranial aneurysm (UIA) samples under varied conditions. The correlation and differences of immune cell types across groups were examined. TF-target genes were obtained from the hTFtarget database, five immune-related TFs were identified and their expression was normalized and validated in an IA mouse model via qRT-PCR and Western blot analysis.

Results: 1852 up-regulated and 971 down-regulated DEGs in Control vs RIA, 583 up-regulated and 389 down-regulated genes in Control vs UIA groups. Most DEGs enriched in immune response, such as circulating immunoglobulin, immunoglobulin mediated immune response and B cell mediated immunity. A TF-target regulatory network of these DEGs were predicted and suggested that TF RUNX3 has the most target genes, including SBDS, ARTN, LTA, GMFB and so on. qRT-PCR and Western blot validated the higher expression of DBP, NR3C2 and ZNF711, and lower expression of RUNX3 and ZFN711 in IA mice.

Conclusion: 5 key TFs DBP, RUNX3, SPIB, NR3C2 and ZNF711 were found to be related to immune response and their up/down-regulated expression were observed in IA mice. As RUNX3, SPIB and NR3C2 shared common target genes, they may involved in co-regulated pathway during IA progression.

Keywords: intracranial aneurysm, immune infiltration, transcriptional factor, TF-target regulatory mechanism

Introduction

Intracranial aneurysms (IA) have an estimated prevalence of 3–5% in the general population worldwide.[1] In China, a study found a prevalence of approximately 5.2% based on an imaging screening study.[2] Despite the high morbidity and mortality rates associated with aneurysm rupture, there is currently no standard population-based screening practice. Diagnosis is typically performed incidentally or after rupture using CT angiography and other imaging modalities, which have inherent limitations.[3–6] Although clipping and coiling procedures have advanced, they still carry procedure-related risks and do not address the underlying disease pathogenesis. There is a clear need for less-invasive pharmacological therapies to stabilize aneurysm progression and prevent rupture.[7]

A mount of previous researches highlight the transcription factors (TFs) such as NF-kB, Ets-1, and Sox17 implicated in the pathogenesis of aneurysms by regulating the inflammatory pathways.[8,9] Decoy oligonucleotides targeting NF-kB

Received: 13 November 2024
Accepted: 24 April 2025
Published: 15 May 2025

Graphical Abstract

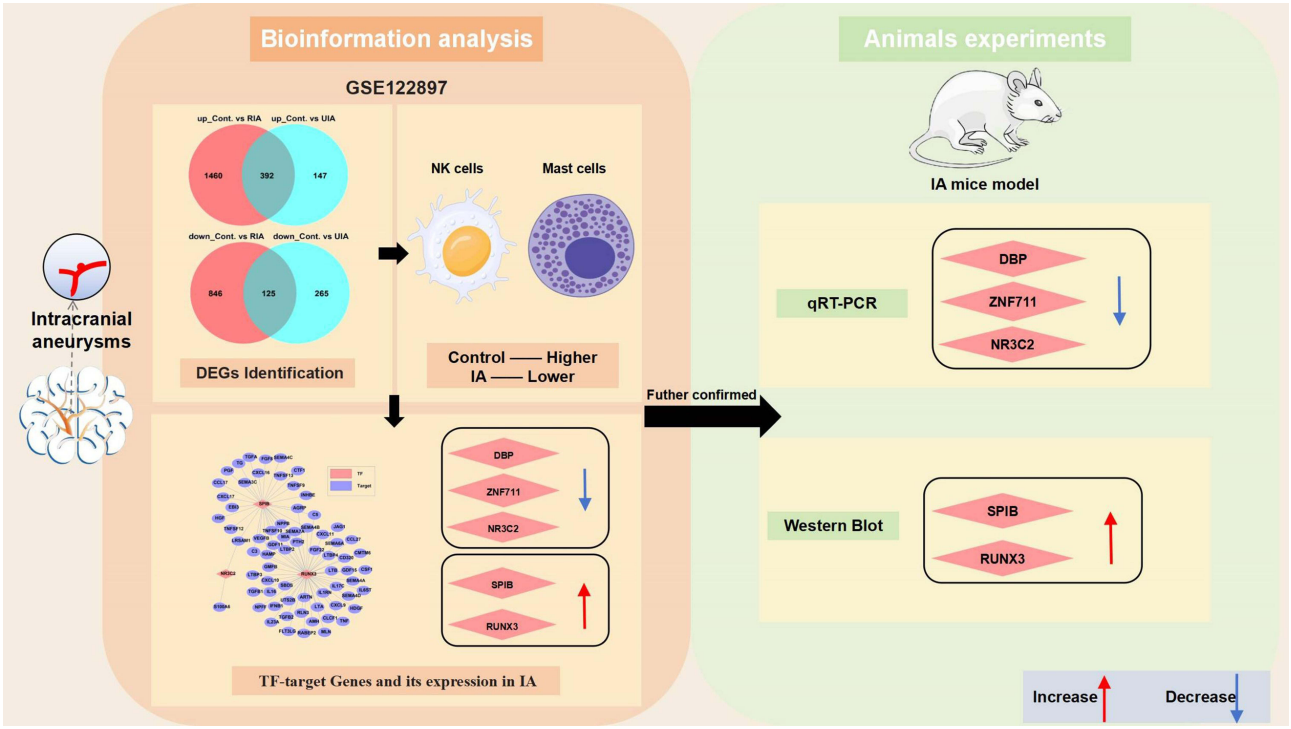

and Ets-1 induce regression of experimentally induced aneurysms in rats (Aoki et al, 2012). Sox17 deficiency led to aneurysm formation in a mouse model (Lee et al, 2015). While demonstrating the pathogenic mechanisms, these TFs studies need to be advanced to include patient populations and potential therapies. The roles of numerous other transcription factors such as RUNX3, SPIB and NR3C2 require further investigation. RUNX3, As one of the RUNX transcription factor family member, play a crucial role in signal transduction pathways in vascular remodeling, endothelial function, immune response and inflammation.[10,11] However, the research on transcription factors such as RUNX3, in intracranial aneurysms remains preliminary, with substantial work needed to determine their functional implications and develop molecular treatments that target regulatory pathways.

Besides, the immune system is also increasingly being implicated in the formation, progression, and rupture of IAs. Multiple studies have demonstrated the infiltration and polarization of macrophages in IA lesions, which can modulate extracellular matrix remodeling and inflammation through cytokine secretion.[12,13] Several studies have revealed the presence of active inflammatory responses in the pathogenesis of IAs, such as macrophage infiltration.[14] Inflammation actively participates in the initiation, progression, and rupture of IAs, which are chronic inflammatory diseases regulated by a positive feedback loop.[15] Genetic studies also support roles for immune-related pathways in IA pathogenesis.[16,17] Additionally, a higher abundance of immune cells and immune pathway activity has been found in ruptured IAs than in unruptured samples.[18,19] Although these findings demonstrate immune involvement, the specific mechanisms by which different immune cells and signals contribute to the development of IA remain unclear. Furthermore, translation of immune-targeted therapies to patients is still lacking. More in-depth characterization of IA immunopathology through multi-omics data and preclinical testing is required.

Publicly available Gene Expression Omnibus (GEO) databases provides transcriptomic data to elucidate the mechanisms of IA formation. Studies have identified key immune-related and functional pathways, networks, and hub genes from GEO datasets of IA and control tissues.[20,21] However, further database mining is required to clarify immune cell type expression, transcription factor regulation, and therapeutic targets. In addition, inconsistencies exist between the

datasets, requiring an integrated analysis. Standardizing computational workflows for GEO data can enhance the reproducibility and collective knowledge. While offering biological insights, findings from database studies need to be validated in clinical samples. Overall, GEO resources show utility for hypothesis generation in IA but have limitations that need to be addressed through multi-platform investigation and wet lab work. In this study, we focused on RNA-seq data from RIA and UIA samples sourced from GEO dataset GSE122897. Through expression profiling, a series of DEGs were identified, and gene function analyses revealed that they were mostly enriched in the immune response. Additionally, five key immune-related TFs were investigated, and the construction of IA mice validated their differential expression patterns. These results can enhance the knowledge about the pathogenesis of aneurysms and identify new treatment strategies.

Materials and Methods

Data Source

Raw data were selected and downloaded from the Gene Expression Omnibus database (GEO; https://www.ncbi.nlm.nih.gov/geo/). RNA-seq profiling datasets were found under accession GSE122897, including 16 control arteries, 22 ruptured IAs (RIAs), and 21 unruptured IAs (UIAs) (Approval number: 2025020701).

Differential Expression Analysis

First, samples were grouped according to their information. Second, RNA-seq datasets were analyzed using the R package edgeR[22] and the Limma package[23] was used to calculate and normalize the obtained chip expression data. Then, the DEGs were obtained with a threshold of |fold change| (FC) > 2 and a p value < 0.05.

Venn Analysis

Overlapped genes of different comparative DEGs were obtained by VennDiagram package[24] for subsequent analysis.

Gene Function Enrichment Analysis

Based on the database of gene ontology (GO),[25] the database of biochemical pathways, and the KEGG pathway database,[26] candidate genes were used to conduct functional enrichment. A statistical algorithm (Fisher's exact test) was used to determine which specific functional items were most closely related to a group of genes. Each item in the analysis results corresponds to a *p*-value that represents significance. The smaller the *p*-value, the greater is the relationship between the item and input genes; that is, most of the genes in the group have the function described by the term.

Immune Infiltration Analysis

According to the gene expression signature of specific cells, CIBERSORT[27] can estimate the scores of specific cells in the expression profile of mixed cells using a deconvolution algorithm. Using the characteristic expression profiles of 22 immune cells provided by the CIBERSORT official website, Wilcoxon test was used to test the differences in immune scores in different groups based on the GSE122897 expression profile. We also visualized the relative proportions of the 22 immune cells using bar graphs. In addition, according to the correlation between the scores of each of the 22 types of immune cells, the samples and immune cells were clustered and visualized using heat maps.

TF Target Gene Regulatory Network

First, TFs in overlapping DEGs and their corresponding target genes were determined according to the hTftarget[28] database. We then identified TF target genes in the immune-related genes of the import.[29] Finally, Cytoscape V3.8 was used to build a TF target gene regulatory network.

Animals

Male C57BL/6J mice, aged 8–10 weeks, were procured from Guangzhou Vital River Laboratory Animal Technology Co., Ltd. The animals were housed under specific pathogen-free (SPF) conditions at the animal facility of the Affiliated Hospital of Youjiang Medical College for Nationalities. The environment provided to these mice was meticulously controlled, ensuring optimal temperature, humidity, and a 12-hour light/dark cycle to mimic natural conditions and promote their well-being. The mice had access to a nutritionally balanced diet and clean water ad libitum, which facilitated health and welfare. The care and use of these animals strictly adhered to the National Regulations for the Administration of Affairs Concerning Experimental Animals. This commitment to animal welfare ensured that the mice were not only maintained in a healthy and stress-free environment but that their use in research was justified and humane. All experimental procedures involving these animals were performed in compliance with the guidelines set forth by the Medical Ethics Committee of the Affiliated Hospital of Youjiang Medical College for Nationalities (approval number: YYFY-LL-2022-66). This oversight ensured that all animal-related activities were conducted responsibly, ethically, and in accordance with the highest standards of animal care.

Construction of IA Mice Model

C57BL/6J mice were divided into two groups (n = 10 each). All mice underwent unilateral (left) nephrectomy. Each mouse had a DOCA (Deoxycorticosterone acetate) pellet (Innovative Research of America, Sarasota, USA) subcutaneous injection, weighing approximately 50 mg/day. Concurrently, the drinking water of the mice was supplemented with 1% NaCl and a high-salt diet was initiated to further augment hypertensive conditions. Tail artery systolic blood pressure (SBP) was measured using the noninvasive tail cuff method to confirm the success of the hypertension model (SBP $\geq$ 140 mmHg). This process can induce systemic hypertension by activating renin-angiotensin system (RAS) and increase intracranial vascular shear stress.[30] For the IA group, elastase, at a meticulously calculated dose of 2 μL of 35 U/mL, was injected into the lateral ventricle of the brain, take bregma as the origin, the coordinates range were AP = −0.5 mm, ML = +1.0 mm, DV = −1.5 mm. It directly destroys the elastin of blood vessels in the brain, simulates the degeneration of blood vessel wall and promotes the formation of aneurysms.[31] In contrast, the sham surgery group received an equivalent volume of saline instead of elastase as the control.[32] After 3 weeks of the experiment, the survival rate of the mice was assessed. Blood pressure was measured by femoral artery intubation under general anesthesia before the end of the experiment.

qRT-PCR

The mice were euthanized, the head of the mice was fixed on the ice box, the skin was cut along the coronal suture, the periosteum was removed, and the skull was exposed. A micro bone drill (about 1 mm diameter) was used to drill holes into both temporal bones (reference coordinates: AP = +1.5 mm, ML = ±2 mm). Remove the bone and gently press with a wet cotton ball to protect the brain tissue. Carefully cut the dura, separating the cerebral hemispheres along the midline, exposing the basilar artery and its branches. Observe the location of the aneurysm (usually distal to the basilar artery or near the perforating vessel). Under a stereoscopic microscope (4x-20x objective), the peripheral nerve tissue was carefully separated along the root of the aneurysm with micro tweezers. Try to preserve the intact aneurysm structure (including endovascular cortex, smooth muscle layer and elastic membrane). Total RNA was extracted from the cerebral arteries of both IA-afflicted and normal mice using TRIzol^{TM} reagent (#15596026, Invitrogen, Carlsbad, CA, USA). RNA purity was assessed by reverse transcribed into complementary DNA using a High-Capacity cDNA Reverse Transcription Kit (#RK21400; Abclonal, USA). Quantitative real-time PCR (qRT-PCR) was performed using an SYBR Green PCR Kit (#204145, Qiagen, Hilden, Germany). mRNA expression levels were quantified using the $2^{-\Delta\Delta Ct}$ method, with β-actin serving as the internal control. Primers used in this study are listed in Table 1.

Western Blot

Proteins extracted from cerebral artery cell lysates of both IA-affected and normal mice were quantitatively analyzed using a BCA kit (#23227, Pierce, Massachusetts, USA). After quantification, the proteins were separated by SDS-PAGE

Table 1 Primers' Sequences of the Genes

DBP	Forward	5′-ACGCACTTTGCCTTTCGG-3′
	Reverse	5′- CTCTTGGCTGCTTCATTGTTCT-3′
NR3C2	Forward	5′-CCTTTCCGCCTGTCAATG-3′
	Reverse	5′-GTCCTTCCACGGCTCTTT-3′
RUNX3	Forward	5′-GCAACGCTTCCGCTGTCA-3′
	Reverse	5′-GTCAAACTGGCGGGGGTCGGAGAAG-3′
SPIB	Forward	5′-CAGAGGACTTCACCAGCCAGAC-3′
	Reverse	5′-AGCGGCGAGCCAACAACT −3′
ZNF711	Forward	5′-TTACGAAACTGCCGAACA-3′
	Reverse	5′-GCTCTGAAGGACGATGAA-3′
β-actin	Forward	5′-GTCCCTCACCCTCCCAAAAG-3′
	Reverse	5′-GCTGCCTCAACACCTCAACCC-3′

and transferred to PVDF membranes (#IPVH00010, Millipore, USA). Membranes were then incubated with a series of primary antibodies: anti-DBP (#12662-1-AP, Proteintech, China), anti-RUNX3 (ab135248, Abcam, UK), anti-SPIB (#14337, Cell Signaling Technology, USA), anti-NR3C2 (#ab64457, Abcam, UK), anti-ZNF711 (#16823725, Fisher Scientific), and anti-β-actin (ab213262, Abcam, UK). Subsequently, the membranes were incubated with an HRP-conjugated secondary antibody (Goat Anti-Rabbit IgG H&L HRP, ab205718; Abcam, UK). Chemiluminescent detection was performed using a ChemiDoc MP imager (Bio-Rad, USA), providing detailed visualization of the protein bands on PVDF membranes.

Statistical Analysis

Statistical analyses were performed using the GraphPad Prism V.9.5.1. Independent experiments were performed at least three times, and the results are presented as mean ± SD. Two groups were compared using Student's *t*-test, whereas multiple groups were compared using one-way ANOVA. $p < 0.05$.

Results

DEGs Identification

To elucidate the potential biological mechanisms predisposing patients to IA rupture, 1852 upregulated genes and 971 downregulated genes were identified in the GSE122897 dataset (control vs RIA). Similarly, 583 upregulated and 389 downregulated genes were identified in the GSE122897 dataset (control vs UIA). The volcano map clearly shows the location of DEGs by FC and *p* value in control vs RIA and control vs UIA (Figure 1A and B). Overlapping analysis of the up/down-regulatory genes between the control vs RIA and Control vs UIA groups was carried out. There were 392 upregulated and 125 downregulated common DEGs between Control vs RIA and control vs UIA groups, respectively (Figure 1C). We plotted a heatmap of the first 20 DEGs sorted in order of $\log_2$FC from the control vs RIA samples (Figure 1D), which showed two main clusters. One cluster included genes upregulated in control samples and down-regulated in RIA samples, whereas the other cluster consisted of genes upregulated in RIA samples and downregulated in control samples. Similarly, the same two clusters were observed in the control vs UIA groups (Figure 1E). Notably, the DEGs in Control vs RIA group were not the same as those in the control vs UIA group.

Gene Function Enrichment Analyses

GO and KEGG enrichment analyses of above overlapped DEGs were next performed to decipher their important function and find out key possible regulatory genes. GO contained three categories: biological processes (BP), molecular functions (MF), and cellular components (CC). From the GO-CC results, terms "Plasma membrane", "Immunoglobulin complex, circulating" and "Integral component of plasma membrane" were the top 3 pathway been enriched (Figure 2A); From the GO-MF results, "Immunoglobulin receptor binding", "Ion transmembrane transporter activity" and "Metal ion transmembrane transporter activity" were the top 3 pathway been enriched (Figure 2B); From the GO-BP results, terms

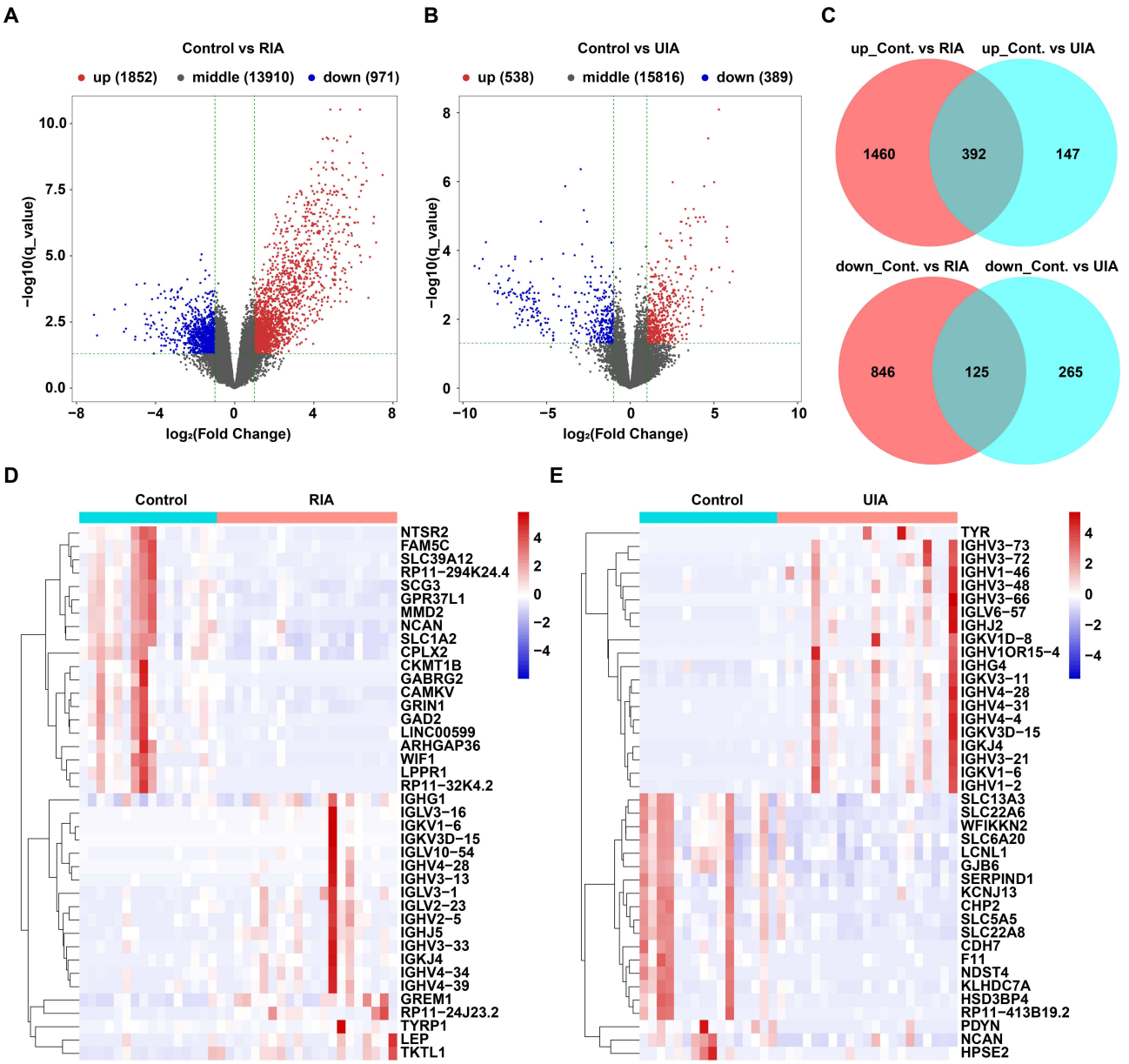

Figure 1 Differential expression analysis. (**A**) Volcano map of DEGs between Control vs RIA group. (**B**) Volcano map of DEGs between Control vs UIA group. (**C**) The venn diagram of up- and down-regulated overlapped genes between Control vs RIA and Control vs UIA groups. (**D**) Heatmap of first 20 DEGs between Control vs RIA. (**E**) Heatmap of first 20 DEGs between Control vs RIA. In Figure 1A and 1B, the x axis in the map is the fold change of gene expression rates between the two samples (with logarithmic treatment), and the y axis is the statistical test value, ie, q value. The higher -log10 (q value) was, the more significant the difference was. Each dot in the graph represents a specific gene, the red dot indicates the significantly up-regulated gene, the blue dot indicates the significantly down regulated gene, and the gray dot indicates no significant difference gene.

"complement activation, classical pathway", "humoral immune response mediated by circulating immunoglobulin" and other key terms were enriched (Figure 2C). The enriched GO-BP terms were related to DEGs containing IGHV4-34, IGHV4-28, IGLV3-1, IGLV2-23 and so among others (Figure 2D). As for KEGG pathways, the pathways "Calcium signaling pathway", "Cocaine addiction", "cAMP signaling pathway" and other some pathways were enriched (Figure 2E), genes SLC6A3, COL10A1, COL1A2 and IL6 involved in enriched KEGG pathways may play a crucial role in IA (Figure 2F).

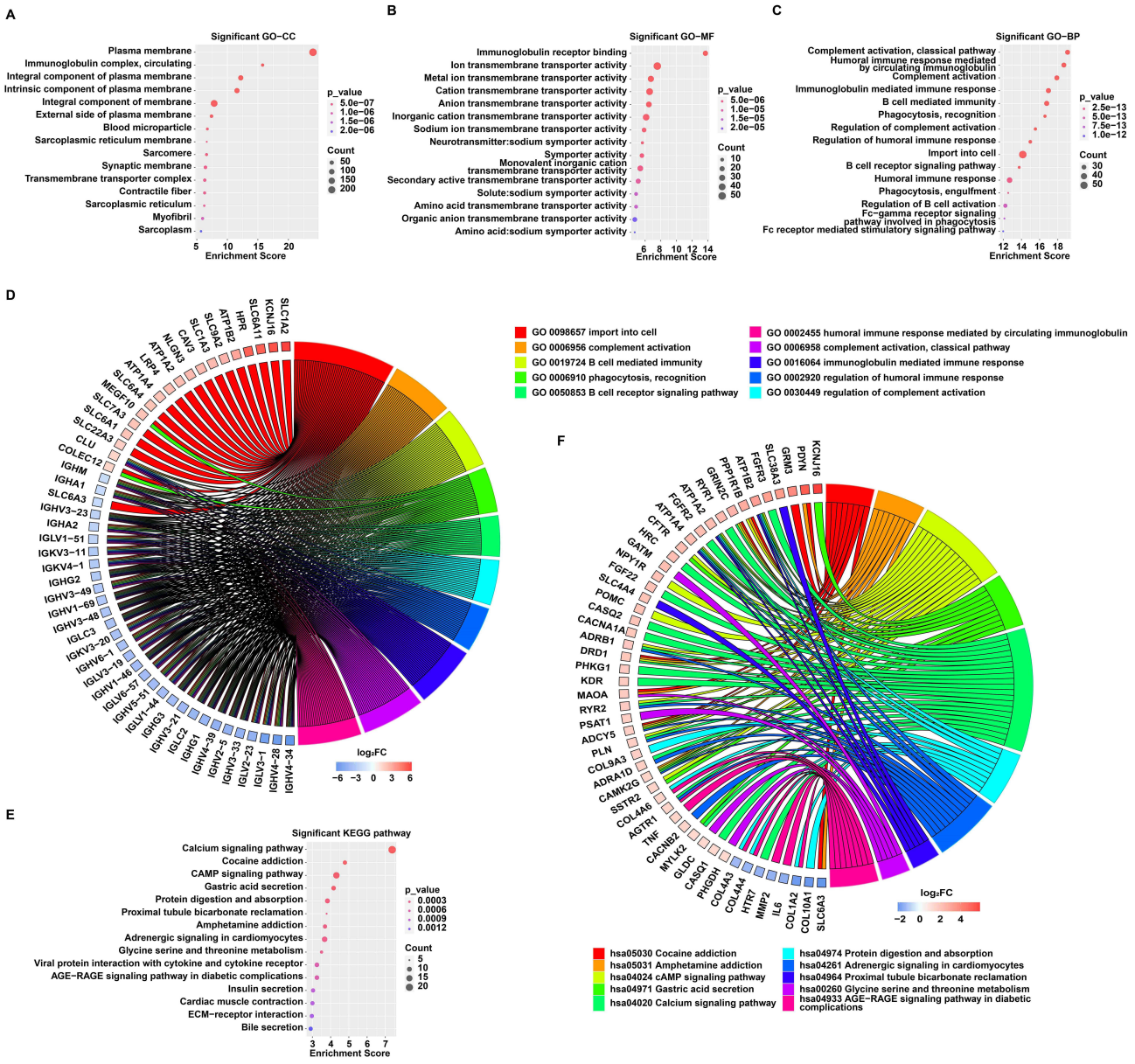

Figure 2 Gene function enrichment analyses results of overlapped genes Bubble chart of the top 15 (**A**) GO-CC terms, (**B**) GO-MF terms and (**C**) GO-BP terms ranked in the enrichment score. (**D**) Circle diagram of GO-BP results covering top 10 significant GO terms ranked in absolute log_2FC values. (**E**) Bubble chart of the top 15 GO-CC terms ranked in the enrichment score. (**F**) Circle diagram of KEGG gene enrichment results covering top 10 significant KEGG pathways ranked in absolute log_2FC values. Within 4 bubble charts, the vertical axis represents GO term or KEGG pathway, and the horizontal axis represents enrichment score. The larger the value, the greater the enrichment degree. The size of the point indicates the number of genes in the GO term or KEGG pathway, and the color of the point corresponds to different *p*-value ranges.

Infiltrating Scores of Differential Immune Cell Populations

Based on the expression of each gene in the GSE122897 dataset, CIBERSORT was used to predict and score the immune cell composition of each sample and to analyze the types of immune cell subpopulations using the Wilcoxon test (Figure 3). First, the differential immune cell subpopulations were clustered by score (Figure 3A and B). Most immune cell subsets in the control vs RIA or Control vs UIA groups showed no differential expression. Activated mast cells (p = 0.001) and activated NK cells (p = 0.004) had significantly higher scores in the control group than in the RIA group, whereas activated NK cells (p = 0.044) and resting NK cells (p = 0.044) had significantly higher scores in the control group than in the UIA group (Figure 3C and D).

https://doi.org/10.2147/JIR.S506360

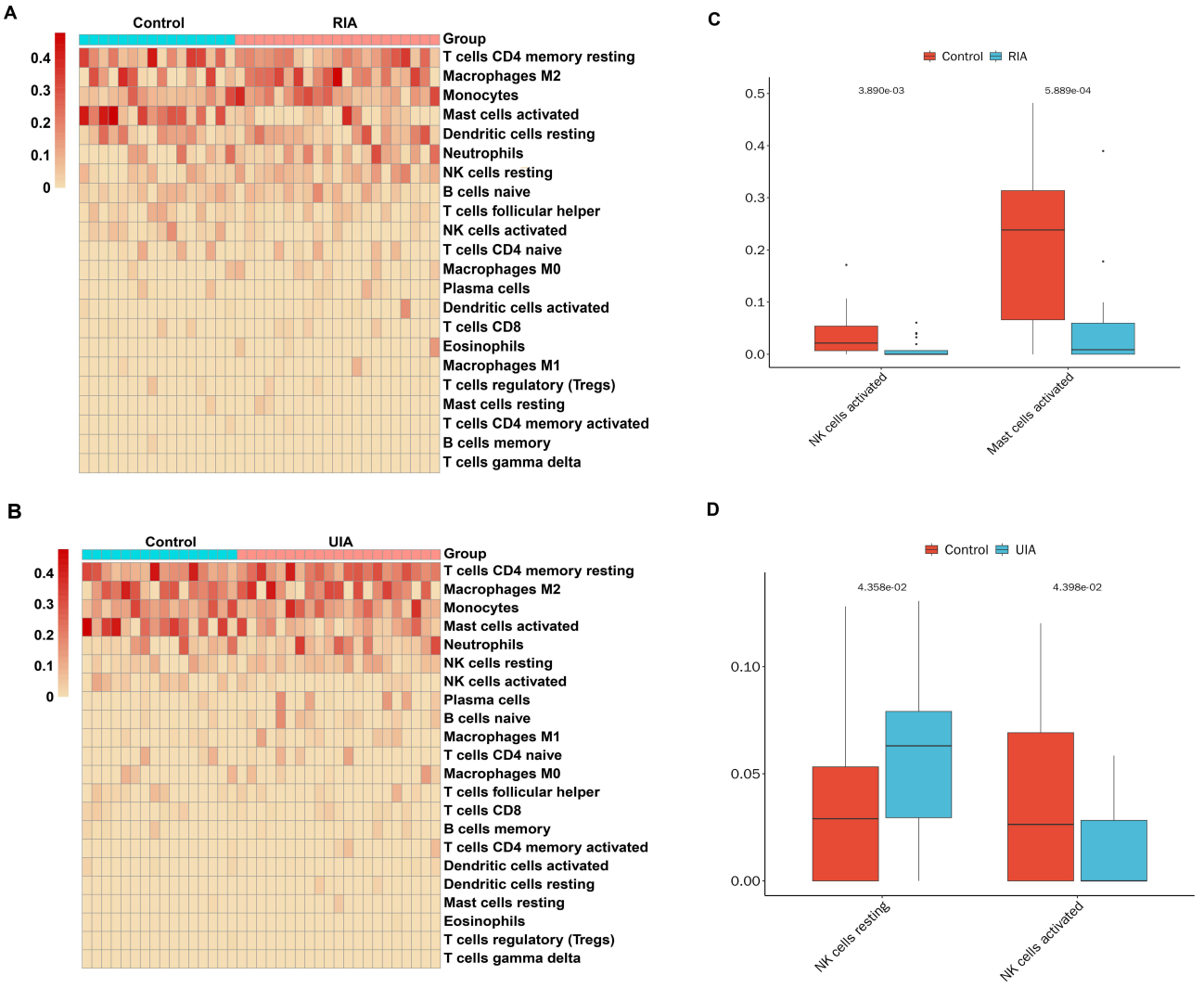

Figure 3 Immune infiltration analysis of differential immune cell populations. Heat map of 22 immune cell scores of each sample from (**A**) Control and RIA samples and (**B**) Control and UIA samples. Box plot of the fraction of immune cells which have significant difference in different groups of (**C**) Control and RIA samples and (**D**) Control and UIA samples.

Construction of TF-Target Network

Using the hTFtarget database, we selected TFs from overlapping genes (Figure 1C), identified their target genes, and filtered them to select those associated with immunity using the ImmPort database. Finally, a TF target gene network was constructed using Cytoscape software. Because DBP and ZNF711 do not have target genes related to immunity based on the ImmPort database, only RUNX3, SPIB, and NR3C2 are shown in the TF target regulatory network (Figure 4). RUNX3, SPIB, and NR3C2 regulate different numbers of target genes related to immunity, based on the ImmProt database. Interestingly, these target genes were identified as DEGs. The node RUNX3 in the TF-target network showed the highest degree; that is, among these three TFs, RUNX3 had the highest number of target genes, including SBDS, ARTN, LTA, and GMFB. In this TF-target network, some shared target genes were found. For example, NR3C2 possessed only two target genes, one of which was targeted by SPIB.

Validation of 5 TFs from DEGs

As shown in Figure 5A and B, we normalized the expression values of the five TFs and plotted violin diagrams based on the GSE122897. DBP, NR3C2 and ZNF711 had significantly lower expression levels in both 22 RIA and 21 UIA

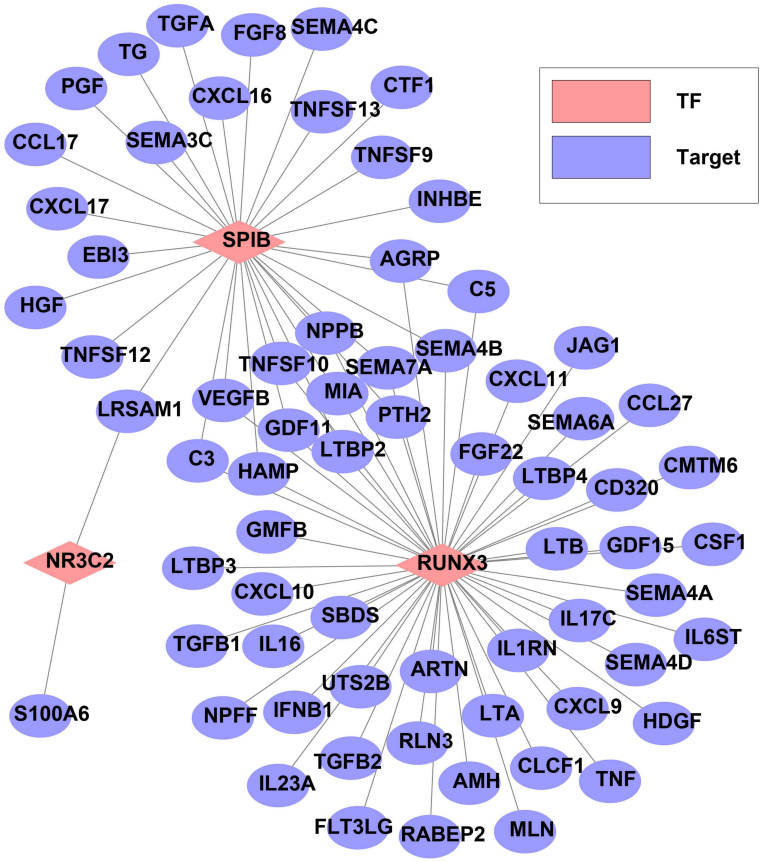

Figure 4 TF-target regulatory network. The red diamond indicates TFs, whereas the blue circle represents target genes.

samples compared to the control group, in view of RUNX3 and SPIB, they showed significantly higher expression than the control group.

An IA mouse model was used to validate the reality and robustness of the five TFs. Total RNAs and protein were extracted from the cerebral arteries of IA and normal mice, qRT-PCR and Western blotting were performed. Consistent with the results of the expression profiling, DBP was significantly down-regulated in IA mice, as well as NR3C2 and ZNF711, whereas RUNX3 and SPIB showed the opposite pattern (Figure 5C and D).

Discussion

IAs are pathological dilations in major branching brain arteries that affect 3–5% of the adult population.[33] Rupture of an IA results in subarachnoid hemorrhage (SAH), which has a poor outcome in up to 35% of the patients.[34] More robust data is needed to gain a deeper understanding of IA mechanisms, and to explore more effective and safety therapies. In this study, we associated IA with the regulation of TFs and their targets, particularly TFs associated with immune infiltration. DEGs in RIA and UIA samples were identified, and functional enrichment analysis results suggested that these DEGs were related to many immune response processes, such as the humoral immune response mediated by circulating immunoglobulins, immunoglobulin-mediated immune response, and B cell-mediated immunity. Further immune infiltration analysis revealed four significantly different immune cell subpopulations, which may be involved in IAs formation or rupture. Five immune-related TFs were selected for the construction of a TF-target network, and their expression was validated through the co-analysis of another dataset and independent experiments. Similar researches were also reported before, but the key TFs were difference from our study. Shengjie Li et al explored the role of immune infiltration in the pathogenesis of IAs, They identified 10 hub genes related to immune, 2 TFs (YY1, GATA2) were also identified, which were the main regulatory factor of hub genes.[35] Besides, Lvyin Luo et al found two key hub genes

https://doi.org/10.2147/JIR.S506360

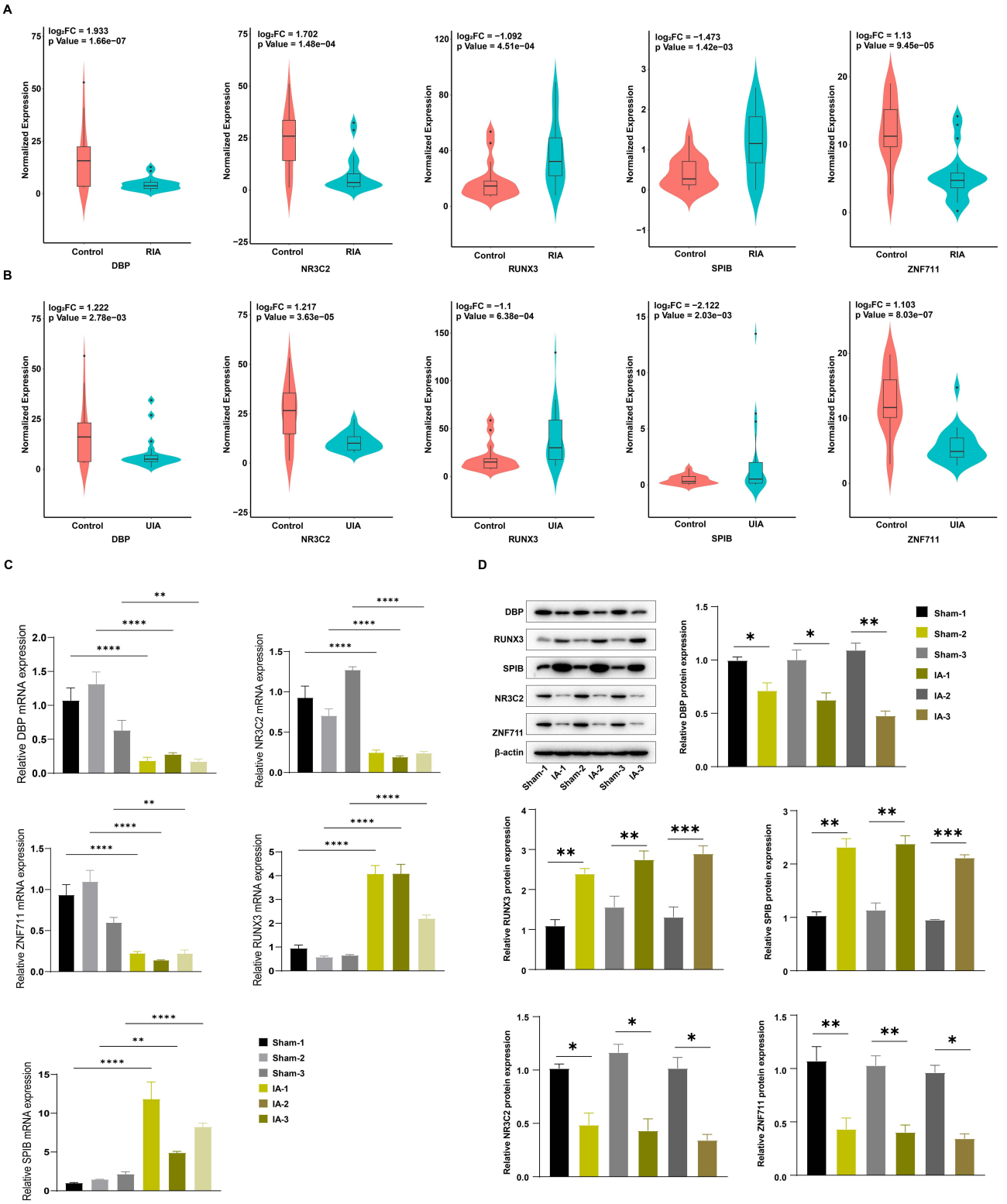

Figure 5 Validation of differentially expressed TF in RIA and UIA samples. Violin diagram of normalized expression of 5 TFs in (**A**) RIA and (**B**) UIA samples. (**C**) mRNA and (**D**) protein levels of 5 TFs in IA and normal mice. *p ≤ 0.05; **p ≤ 0.01; ***p ≤ 0.001, ****p ≤ 0.0001.

https://doi.org/10.2147/JIR.S506360

related to immune (TLR4, ALOX5) in IA, and these two genes would be the a promising therapeutic target for IA.[36] Especially, the RUNX3, SPIB, and NR3C2 did not found to be research deeply in IAs.

An increasing body of research suggests that inflammation of the aneurysm wall may play a pivotal role in the growth and rupture of IAs.[37,38] In a study involving 108 IAs in 87 patients, inflammation around the aneurysm wall was found to be associated with aneurysm growth or rupture through MRI visualization.[39] In another study involving 22 IA patients (30 IAs), researchers found increased infiltration of inflammatory marker macrophages in seven IAs, which suggests elevated levels of inflammation in the aneurysm wall.[40] In our study, although immune infiltration analysis showed that activated mast cells ($p = 0.001$) and activated NK cells ($p = 0.004$) significantly changed in the control vs RIA group, activated NK cells ($p = 0.044$) and resting NK cells ($p = 0.044$) had significantly higher scores in the control group than in the UIA group. Mast cells induce inflammation by releasing a series of bioactive substances such as histamine, lipid mediators, and cytokines, leading to vasodilation, increased permeability of blood vessels, and attraction of other immune cells. On the other hand, NK cells primarily exert regulatory control over inflammation through the recognition and elimination of abnormal or infected cells, as well as the production of immunomodulatory molecules. Our results indicate that inflammation may occur during IAs progression, and there were some differences in the inflammatory response before and after IAs rupture.

All five immune-related TFs showed significant differential expression in both RIA and UIA samples and their robustness was validated in animal experiments. Among these five TFs, RUNX3, SPIB, and NR3C2 shared common target genes, such as AGRP, C5, SEMA4B, C3, VEGFB, LRSAM1 and so forth. The presence of these common target genes suggests a co-regulatory role for RUNX3, SPIB, and NR3C2 in various biological processes, including immune response, neural development, metabolism, and intracellular biology. In-depth research on these genes and their regulatory mechanisms may contribute to a better understanding of IA formation and progression.

Conclusion

Through expression profiling of RNS-seq data in the GSE122897 dataset, we identified DEGs in RIA and UIA samples. Gene function enrichment analysis revealed that immune response was the most enriched. Five immune-related TFs were identified in the present study. RUNX3 and SPIB showed higher expression levels in IA samples, whereas DBP, NR3C2 and ZNF711 showed opposite patterns.

Abbreviation

IAs, Intracranial aneurysms; DEGs, differential expression genes; TFs, Transcription factors; GEO, Gene Expression Omnibus; GO, gene ontology; SPF, specific pathogen-free; qRT-PCR, Quantitative real-time; BP, biological processes; MF, molecular functions; CC, Cellular components; SAH, subarachnoid hemorrhage; RIAs, ruptured IAs; UIAs, unruptured IAS.

Data Sharing Statement

Data sourced from the Gene Expression Omnibus (GEO) and The Cancer Genome Atlas (TCGA) databases.

Ethical Approval

This study adhered to ethical standards and was approved by the Medical Ethics Committee of the Affiliated Hospital of Youjiang Medical College for Nationalities (approval number: YYFY-LL-2022-66, 2025020701).

Author Contributions

All authors made a significant contribution to the work reported, whether that is in the conception, study design, execution, acquisition of data, analysis and interpretation, or in all these areas; took part in drafting, revising or critically reviewing the article; gave final approval of the version to be published; have agreed on the journal to which the article has been submitted; and agree to be accountable for all aspects of the work.

Funding

This study was supported by the Guangxi Natural Science Foundation (2024GXNSFAA010106) and The First Batch of High-level Talent Scientific Research Projects of the Affiliated Hospital of Youjiang Medical University for Nationalities in 2019 (R20196315).

Disclosure

The authors declare that there are no competing interests associated with the manuscript.

References

1. Kataoka H. Molecular mechanisms of the formation and progression of intracranial aneurysms. *Neurologia medico-chirurgica*. 2015;55(3):214–229. doi:10.2176/nmc.ra.2014-0337
2. Yu SC, Cheng P, Antonio GE, Chan SC, Lau TW, Ma HT. Prevalence of unruptured intracranial aneurysms in the Hong Kong general population and comparison with individuals with symptoms or history of cerebrovascular disease. *Hong Kong Med J*. 2022;28(1):16–23. doi:10.12809/hkmj209236
3. Lozano CS, Lozano AM, Spears J. The changing landscape of treatment for intracranial aneurysm. *Can J Neurol Sci*. 2019;46(2):159–165. doi:10.1017/cjn.2019.7
4. Hall JM, McElroy BJ, Arora PK, Mohandas S. Intracranial mycotic aneurysm complicating streptococcus pneumoniae infection. *J Pediatr*. 2019;211:223–223.e221. doi:10.1016/j.jpeds.2019.03.031
5. Zhang D, Wang H, Liu T, Feng Y, Qi Y, Xu N. Re-recurrence of intracranial aneurysm with proximal vascular stenosis after primary clipping and secondary endovascular embolization: a case report and literature review. *World Neurosurg*. 2019;121:28–32. doi:10.1016/j.wneu.2018.09.088
6. Hussein AE, Brunozzi D, Shakur SF, Ismail R, Charbel FT, Alaraj A. Cerebral aneurysm size and distal intracranial hemodynamics: an assessment of flow and pulsatility index using quantitative magnetic resonance angiography. *Neurosurgery*. 2018;83(4):660–665. doi:10.1093/neuros/nyx441
7. Aoki T, Frösen J, Fukuda M, et al. Prostaglandin E2–EP2–NF-κB signaling in macrophages as a potential therapeutic target for intracranial aneurysms. *Sci Signaling*. 2017;10(465):eaah6037. doi:10.1126/scisignal.aah6037
8. Aoki T, Kataoka H, Nishimura M, Ishibashi R, Morishita R, Miyamoto S. Regression of intracranial aneurysms by simultaneous inhibition of nuclear factor-κB and Ets with chimeric decoy oligodeoxynucleotide treatment. *Neurosurgery*. 2012;70(6):1534–1543. doi:10.1227/NEU.0b013e318246a390
9. Lee S, Kim I-K, Ahn JS, et al. Deficiency of endothelium-specific transcription factor Sox17 induces intracranial aneurysm. *Circulation*. 2015;131(11):995–1005. doi:10.1161/CIRCULATIONAHA.114.012568
10. Dubis J, Litwin M, Michalowska D, et al. Elevated expression of runt-related transcription factors in human abdominal aortic aneurysm. *J Biol Regul Homeost Agents*. 2016;30(2):497–504.
11. Chuang LSH, Matsuo J, Douchi D, Bte Mawan NA, Ito Y. RUNX3 in stem cell and cancer biology. *Cells*. 2023;12(3):408. doi:10.3390/cells12030408
12. Wang Y, Jin J. [Roles of macrophages in formation and progression of intracranial aneurysms]. *Zhejiang da xue xue bao Yi xue ban*. 2019;48(2):204–213. doi:10.3785/j.issn.1008-9292.2019.04.13 Danish
13. Muhammad S, Chaudhry SR, Dobreva G, Lawton MT, Niemelä M, Hänggi D. Vascular macrophages as therapeutic targets to treat intracranial aneurysms. *Front Immunol*. 2021;12:630381. doi:10.3389/fimmu.2021.630381
14. Yang Q, Yu D, Zhang Y. β-Sitosterol attenuates the intracranial aneurysm growth by suppressing TNF-α-mediated mechanism. *Pharmacology*. 2019;104(5–6):303–311. doi:10.1159/000502221
15. Shimizu K, Kushamae M, Mizutani T, Aoki T. Intracranial aneurysm as a macrophage-mediated inflammatory disease. *Neurologia medico-chirurgica*. 2019;59(4):126–132. doi:10.2176/nmc.st.2018-0326
16. Li S, Zhang Q, Weng L, Han Y, Li J. Novel insight into m6A regulator-mediated methylation modification patterns and immune characteristics in intracranial aneurysm. *Front Aging Neurosci*. 2022;14:973258. doi:10.3389/fnagi.2022.973258
17. Turhon M, Maimaiti A, Gheyret D, et al. An immunogenic cell death-related regulators classification patterns and immune microenvironment infiltration characterization in intracranial aneurysm based on machine learning. *Front Immunol*. 2022;13:1001320. doi:10.3389/fimmu.2022.1001320
18. Niu S, Zhao Y, Ma B, et al. Construction and validation of a new model for the prediction of rupture in patients with intracranial aneurysms. *World Neurosurg*. 2021;149:e437–e446. doi:10.1016/j.wneu.2021.02.006
19. Tutino VM, Zebraski HR, Rajabzadeh-Oghaz H, et al. RNA sequencing data from human intracranial aneurysm tissue reveals a complex inflammatory environment associated with rupture. *Mol Diagn Ther*. 2021;25(6):775–790. doi:10.1007/s40291-021-00552-4
20. Guo T, Hou D, Yu D. Bioinformatics analysis of gene expression profile data to screen key genes involved in intracranial aneurysms. *Mol Med Rep*. 2019;20(5):4415–4424. doi:10.3892/mmr.2019.10696
21. Chen S, Li M, Xin W, et al. Intracranial aneurysm's association with genetic variants, transcription abnormality, and methylation changes in ADAMTS genes. *PeerJ*. 2020;8:e8596.
22. Robinson MD, McCarthy DJ, Smyth GK. edgeR: a Bioconductor package for differential expression analysis of digital gene expression data. *bioinformatics*. 2010;26(1):139–140. doi:10.1093/bioinformatics/btp616
23. Ritchie ME, Phipson B, Wu D, et al. limma powers differential expression analyses for RNA-sequencing and microarray studies. *Nucleic Acids Res*. 2015;43(7):e47–e47. doi:10.1093/nar/gkv007
24. Chen H, Boutros PC. VennDiagram: a package for the generation of highly-customizable Venn and Euler diagrams in R. *BMC Bioinf*. 2011;12(1):1–7. doi:10.1186/1471-2105-12-35
25. Ashburner M, Ball CA, Blake JA, et al. Gene ontology: tool for the unification of biology. *Nat Genet*. 2000;25(1):25–29. doi:10.1038/75556
26. Kanehisa M, Goto S. KEGG: Kyoto Encyclopedia of Genes and Genomes. *Nucleic Acids Res*. 2000;28(1):27–30. doi:10.1093/nar/28.1.27

27. Chen B, Khodadoust MS, Liu CL, Newman AM, Alizadeh AA. Profiling tumor infiltrating immune cells with CIBERSORT. *Methods Mol Biol*. 2018 ;1711:243–259. doi:10.1007/978-1-4939-7493-1_12
28. Zhang Q, Liu W, Zhang H-M, et al. hTFtarget: a comprehensive database for regulations of human transcription factors and their targets. *Genom Proteom Bioinf*. 2020;18(2):120–128. doi:10.1016/j.gpb.2019.09.006
29. Bhattacharya S, Dunn P, Thomas CG, et al. ImmPort, toward repurposing of open access immunological assay data for translational and clinical research. *Scientific Data*. 2018;5(1):1–9. doi:10.1038/sdata.2018.15
30. Su C, Xue J, Ye C, Chen A. Role of the central renin-angiotensin system in hypertension (Review). *Int J Mol Med*. 2021;47(6). doi:10.3892/ijmm.2021.4928
31. Strange F, Gruter BE, Fandino J, Marbacher S. Preclinical intracranial aneurysm models: a systematic review. *Brain Sci*. 2020;10(3):134. doi:10.3390/brainsci10030134
32. Yanagisawa T, Zhang H, Suzuki T, et al. Sex and genetic background effects on the outcome of experimental intracranial aneurysms. *Stroke*. 2020;51(10):3083–3094. doi:10.1161/STROKEAHA.120.029651
33. Vlak MH, Algra A, Brandenburg R, Rinkel GJ. Prevalence of unruptured intracranial aneurysms, with emphasis on sex, age, comorbidity, country, and time period: a systematic review and meta-analysis. *Lancet Neurol*. 2011;10(7):626–636. doi:10.1016/S1474-4422(11)70109-0
34. Nieuwkamp DJ, Setz LE, Algra A, Linn FH, de Rooij NK, Rinkel GJ. Changes in case fatality of aneurysmal subarachnoid haemorrhage over time, according to age, sex, and region: a meta-analysis. *Lancet Neurol*. 2009;8(7):635–642. doi:10.1016/S1474-4422(09)70126-7
35. Li S, Xiao J, Yu Z, Li J, Shang H, Zhang L. Integrated analysis of C3AR1 and CD163 associated with immune infiltration in intracranial aneurysms pathogenesis. *Heliyon*. 2023;9(3):e14470. doi:10.1016/j.heliyon.2023.e14470
36. Luo L, Ma X, Kong D, et al. Multiomics integrated analysis and experimental validation identify TLR4 and ALOX5 as oxidative stress-related biomarkers in intracranial aneurysms. *J Neuroinflammation*. 2024;21(1):225. doi:10.1186/s12974-024-03226-0
37. Chalouhi N, Hoh BL, Hasan D. Review of cerebral aneurysm formation, growth, and rupture. *Stroke*. 2013;44(12):3613–3622. doi:10.1161/STROKEAHA.113.002390
38. Hasan DM, Mahaney KB, Brown RD Jr, et al. Investigators ISoUIA: aspirin as a promising agent for decreasing incidence of cerebral aneurysm rupture. *Stroke*. 2011;42(11):3156–3162. doi:10.1161/STROKEAHA.111.619411
39. Edjlali M, Gentric J-C, Régent-Rodriguez C, et al. Does aneurysmal wall enhancement on vessel wall MRI help to distinguish stable from unstable intracranial aneurysms? *Stroke*. 2014;45(12):3704–3706. doi:10.1161/STROKEAHA.114.006626
40. Hasan D, Chalouhi N, Jabbour P, et al. Early change in ferumoxytol-enhanced magnetic resonance imaging signal suggests unstable human cerebral aneurysm: a pilot study. *Stroke*. 2012;43(12):3258–3265. doi:10.1161/STROKEAHA.112.673400